Vertical Changes in the Storm Tracks and Dynamics of Western Disturbances

Vadlamudi Brahmananda Rao
National Institute for Space Research
Henri Pinheiro
National Institute for Space Research
Raju Attada (rajuattada@iisermohali.ac.in)
Indian Institute of Science Education and Research Mohali
V. S. L Bhargavi
Andhra University
S. S.V.S Ramakrishna
Andhra University
Dandu Govardhan
University of Hyderabad
Manoel Alonso Gan
National Institute for Space Research
Ashok Karumuri
University of Hyderabad
Ramesh K J
India Meteorological Department

Research Article

Keywords: Storm tracks, western disturbances, northern hemisphere, baroclinic instability

Posted Date: April 15th, 2022

DOI: https://doi.org/10.21203/rs.3.rs-1551236/v1

Abstract

This study investigates the long-term horizontal and vertical changes of the storm tracks during the1979-2014 period using a cyclone tracking algorithm for all the boreal seasons in the Northern Hemisphere. During winter, the Atlantic and Pacific storm tracks are stronger and remain circumpolar. These winter storm tracks extend meridionally from polar region to 30°N, and vertically extend from the lower troposphere to the lower stratosphere. Characteristically, baroclinic instability is a common mechanism of generation associated with storm tracks and western disturbances (WDs), which often occur in northern parts of India, mostly in fall and winter. We found that observed WDs are generated by moist baroclinic instability of westerlies over Indian longitudes as their characteristics agree well with theoretically and numerically deduced ones. Indeed, these WDs observed during the boreal fall and winter seasons are ingredients of the storm tracks in the northern hemisphere, with strengthened relative vorticity at 500 hPa and moving zonally eastward towards the north Indian region triggering extreme precipitation. Thus, WDs over northern India is of great interest in the fall and winter seasons.

1. Introduction

Winter precipitation is essential for the Kharif & Rabi crops in India. Thus, it is necessary to determine the generation mechanism of western disturbances (WDs), without which a skillful weather forecast can not be obtained. A reliable weather forecast is necessary for agricultural planning. Hunt et al. (2018a) observed three main characteristics of western disturbances: 1) westward vertical tilt, 2) rising motion ahead of the trough axis, and 3) a horizontal wavelength of about 2000 km. These features, particularly in the intermediate horizontal scale, can only be explained by the moist baroclinic instability, systematically deduced by Bonatti and Rao (1987). Dry baroclinic instability, on the other hand, can only explain the generation of large-scale disturbances on the order of 6000 km, as found by Holton (2014). Thus, observed WDs by Hunt et al. (2018a) are, indeed, generated by moist baroclinic instability.

Storm Tracks (STs) have been the subject of several investigations for a long time. STs are the local regions where mid-latitude baroclinic waves develop and decay. Charney (1947) demonstrated for the first time in a seminal paper that baroclinic instability is the cause of mid- and higher- latitude weather-producing storms. In this theoretical study, Charney (1947) used a zonally averaged zonal wind varying with height, so the ensuing results can be applied to zonally symmetric baroclinic disturbances only. However,, Blackmon (1976) showed that STs are regions of storm occurrence that are localized in the observed atmosphere. Their study reported that the distribution of the variance of the bandpass filtered (between 2.5 and 6 days) series was found to be along the North Atlantic and North Pacific STs in winter at 500 hPa level. These STs are the regions that have a high frequency of cyclonic activity, first noted by Sawyer (1970).

Hartman (1974) conducted a spectral analysis study on the vertical variation of observed baroclinic waves in the midlatitudes. This study further discovered that the observed characteristics were very similar to the quasi-geostrophic and hydrostatic baroclinic waves studied by many researchers, including Charney (1947) and Eady (1949). Hartman (1974) further extended his study to the extratropical stratosphere at 100 hPa and observed that baroclinic waves are damped as energy propagates into the stratosphere. Although the temperature increases towards the pole from lower latitudes in the stratosphere, this damping is caused by the transport of sensible heat to the north, thus, the mean available potential energy increases at the expense of perturbation available potential energy. Thus, these waves maintain the mean temperature gradient in the lower stratosphere.

Later, several authors studied STs in both hemispheres (e.g. Hoskins and Hodges 2002; Wang et al. 2017; Hoskins and Hodges 2019). However, most of the work focuses on the Northern Hemisphere (NH), with much less attention paid to the Southern Hemisphere (SH). Hoskins and Hodges (2002; 2019) presented several observed characteristics at only two vertical levels, namely 250 and 850 hPa. Some of the main characteristics they found are: 1)much of the STs intensity in winter is retained in spring, and there is only a small change in their latitude; 2) they also found the presence of a northern Russian ST at both the levels and in most of the seasons,3) an extension across southern Asia near 30° N may be linked to southern Asia track and possibly related to surface cyclogenesis, and4) the lower troposphere Mediterranean ST is noted in Winter and Spring with increased activity in Spring and possibly related to the enhanced baroclinic activity.. Many studies, including those of Hoskins and Hodges (2002; 2019), dealt only NH STs. However, some recent studies (e.g. Rao et al. 2002; 2003; Hoskins et al. 2005; Ashok et al. 2007; Ashok et al. 2009; Guo et al. 2009; Zang et al. 2018; Da Siva et al.; 2021; Zhang et al. 2020; Machado et al. 2020) focused on the findings of southern hemispheric STs.

During boreal winter, another important synoptic-scale phenomenon embedded in the subtropical Westerly Jet (SWJ) of NH is the Western Disturbances. These WDs are often associated with extreme rainfall and sometimes even snow across the Pakistan and North Indian regions (e.g., Kotal et al., 2014; Dimri et al. 2015; Attada et al. 2020; Nischal et al. 2022). These WDs are formally defined by the India Meteorological Department (IMD) as *"the cyclonic circulation/trough in the mid and lower tropospheric levels or as a low-pressure area on the surface, which occurs in middle latitude westerlies and originates over the Mediterranean Sea, Caspian Sea and the Black Sea and move eastwards across north India"*. Crucially, the common factor for WDs and STs is that these two phenomena are associated with the SWJ at the upper level in NH. Understanding the relationship between these two phenomena will enable us to gain a better understanding of the variations in the meridional heat gradient and heat flux transfer, which is a fundamental feature of general circulation.

The present research focuses on the vertical variation of STs, primarily across the lower stratosphere, which is still underexplored. Another new aspect not previously addressed is the ST associated with WDs in northern India and its surroundings, particularly in light of renewed interest in WD as evidenced by several works (e.g., Dimri et al. 2015; Hunt et al. 2018a, b). The following section 2 provides the details of the data obtained and the methodology used. Section 3 elucidates the physical phenomenon behind STs and WD. Section 4 presents the findings and discussion, and the final section gives the summary and conclusion of this study.

2. Data And Methodology

We used mean sea level pressure (MSLP) data from the ECMWF interim reanalysis (ERA-Interim; Dee et al. 2011) for the cyclonic tracking algorithm (based on Hodges 1994, 1995, 1999) of STs for the period 1979–2014. ERA-Interim is produced using a spectral model with TL255 horizontal resolution (~ 80 km) and 60 vertical hybrid levels with the model top at 0.1 hPa with 1° × 1° spatial resolution. For Eady growth rate (EGR), NCEP-NCAR reanalysis daily data (available at (2.5° × 2.5°) of u-wind, air temperature, and geopotential height at 200 and 850 hPa pressure levels is taken for the same period. Objective feature techniques have been widely used to produce diagnostics on the spatial distribution and frequency of extratropical cyclones. The tracking algorithm used in this study is based on Hodges (1994, 1995, 1999) using minima of both MSLP and relative vorticity, as negative (positive) vorticity is generally associated with cyclonic features in the SH (NH). The use of the two fields allows a contrast to be done between features of different scales. For the vorticity field, which is found to be the preferred field as the large-scale background less influences it, the analysis is performed at multiple pressure levels (1000, 800, 500, 300 and 100 hPa), which allows to examine the vertical structure of the cyclonic features. The tracking is performed on the sphere to avoid biases that can be introduced when using projections. Before tracking is performed, the background field is removed by setting the coefficients for total wavenumbers less than or equal to five to zero. In addition, the data are spectrally filtered using triangular truncation 42 (T42) on a Gaussian grid, as vorticity is a very noisy field, while T63 is used for MSLP as it is a generally smoother field. Finally, the tracks are filtered to retain only the mobile features that last longer than 48h (eight consecutive time steps) and travel at least 10^{o} geodesic (≅1000 km). The tracks are used to compute a wide range of spatial statistics using the spherical kernel method (Hodges 1996), though here, we focus on the track density, which is computed by using a single point from each track that is closest to the estimation point, given in term of number per season per unit area, where area is equivalent to a 5^{o} geodesic radius spherical cap (, $\hat{a}\ddot{O}10^{6}km^{2}$). To calculate the EGR, here, we have converted available air temperature data into potential temperature. The potential temperature and geopotential height data have been used to compute the Brunt-Vaisala frequency between the two levels (200 minus 850hPa). Similarly, vertical shear of zonal wind has been calculated between 200 and 850 hPa pressure levels. The ratio of calculated vertical shear to Brunt-Vaisala frequency has been used to compute the daily time series of Eady Growth Rate at different grid points (as per the formula mentioned below).

Eady Growth Rate (maximum) $$\sigma_E = 0.3098 \frac{|f| \left| \frac{\partial U(z)}{\partial z} \right|}{N}$$

where N→ Brunt-Vaisala Frequency/buoyancy frequency; U(z) is the vertical profile of the eastward wind component, and f is the Coriolis parameter. Finally, the obtained grid wise daily time series has been used to separate seasonal time series (DJF, MAM, JJA, SON) and are further averaged through time for respective seasons.

3. Characteristics Of Storm Tracks And Western Disturbances

Some of the characteristics that the present authors explored here have also been discussed in previous studies, such as Hoskins and Hodges (2019). However, Hoskins and Hodges (2019) examined STs vertical changes for only two levels, 250 hPa and 850 hPa. Here our focus is to expand on the work of Hoskins and Hodges (2019) by analysing more levels in the vertical, including the lower stratosphere at 100 hPa, using a cyclone tracking algorithm. Hoskins and Hodges (2019) noticed a circumpolar ST in the NH at 250 hPa after observing the separation of Pacific and Atlantic STs at 850 hPa. Furthermore, STs are found further north in the boreal summer than in the winter, and STs at 250 hPa are stronger during boreal winter. Similarly, we also found these features in the present study. In the lower troposphere, even at 1000 hPa, the STs over the Atlantic and Pacific are separated because of the local strong baroclinic instability generation features such as the Canadian High and Siberian High generating high northern winds meeting northernward moving very warm southerly wind on the eastward of the Gulfstream and Kuroshio warm currents (Blackmon 1977). Hoskins and Hodges mention some characteristics of STs (2019). There are some other characteristics of STs that can be attributed to WDs that have not been discussed by prior studies. Here we discuss the WDs phenomenon in very detail and also discuss the vertical variations of the strength of the ST, extension, and seasonal variations in the following section of Results and Discussion.

This study is unique in that it discusses the vertical variations of ST characteristics in the vertical from troposphere to the lower stratosphere (100 hPa) during all boreal seasons, as shown in Table 1. Thus, a close examination of Table 1 allows one to get a concise idea of these variations. For example, WDs are not found at mean sea level pressure (MSLP) or 1000 hPa level and are obviously generated at higher levels only, but of course, they are strongest at 500 hPa during winter. A novel observation we found of STs is that they exist in the lower stratosphere, albeit weak. There was no comparison of WD in STs in earlier studies. The WDs are also generated by the baroclinic instability, as first found by Rao and Rao (1971) more than 50 years ago, like the middle and high latitude extratropical cyclones in STs, which are seen in other regions in the Atlantic and Pacific.

Table 1
The spatial extention (in °)of STs at MSLP, 1000 hPa, 800 hPa, 500 hPa, 300 hPa, 100 hPa.

Season	Winter			Spring			Summer			Autumn		
Height	WD	Pacific	Atlantic	WD	Pacific	Atlantic	WD	Pacific	Atlantic	WD	Pacific	Atlantic
MSLP	-	20–30	30°-40°	-	10°-20°	10°-20°	-	10°-20°	20°-30°	-	10°-20° 30°-40° (Russia)	20°-30° 30°-40° (USA)
1000 hPa	-	50°-60°	60°-70°	-	40°-50°	50°-60°	-	30°-40°	50°-60°	-	50°-60° (East)	40°-50° (West)
800 hPa	Middle-East 40°-50° N	50°-60° (extended)	50°-60° (small)	Middle-East 30°-40°	Horse Shoe 30°-40° (West)	Mid Atlantic 30°-40°	-	West 30°-40°	Mid Atlantic 30°-40°	-	West Pacific 50°-60° 40°-50° (Russia)	Mid Atlantic 40°-50°
500 hPa	Strongest 60°-70° N Middle east 50°-60° N	Extended 50°-60°	Mid Atlantic 50°-60°	50°-60° short	50°-60°	40°-50°	-	40°-50°	40°-50° 50°-60° (short)	Further North 40°-50° short center	50°-60°	West 50°-60°
300 hPa with continuous contours over 90° E & 150° E	Middle east 50°-60° N	50°-60°	50°-60°	Middle East 40°-50°, over 90°E 50°-60°	150°E, 50°-60°	Weak 40°-50°	-	Weak 40°-50°	50°-60°	-	50°-60°	40°-50°
100 hPa weak around 30°N from 30°W to 90°E	10°-20° N	Around 30°N from 180°E to East upto 120°W	At high latitudes, ST north of 60°N from 90°W to 90°E 10–20	-	North of 30°N from 90°E to 150°W	Around 30°N Mid Atlantic 10–20	-	North of 30°N from 30°E to 150°W, maximum Russia 20°-30°	Around 60°N shorter than spring season 10°-20°	-	Continuous ST, North of 30°N upto 0° Maxmimum over 180° 20°-30°	-

In an detailed series of articles, Hunt et al. (2018a,b; 2019a,b) and Dimri et al. (2015) made an investigation of WDs. These are needed before any attempt is made to explain the nature of WD theoretically. Hunt et al. (2018a) show a maximum number of STs concentrated in the northwestern parts of India and Pakistan regions, which are the continuation of STs from the western Pacific region - Middle East - Northwestern parts of India and triggering heavy precipitation. This implies that there is a strong local forcing to raise the baroclinic instability (Figs. 2a,b). This needs a detailed study to emphasize the characteristics of the concentrated ST region of Pakistan and India. Here our primary focus is to discuss the ST and their WD association.

In fact, an accomplished atmospheric and oceanic scientist Prof. A. D. Gill, suggests a three-pronged approach to study and predict weather and climate, namely K-Knowledge (observational studies), U- Understanding (to find causal mechanisms of the determined effects theoretically) and finally M- Modeling (approach to deterministic prediction). In the case of WD, mainly K and a little M seem to be done by several researchers. But, U is almost lacking which needs to be focused with the help of observations. In our knowledge the only attemt seemed to be that of Rao and Rao (1971). Here we extend that simple study to explain the physical importance of STs and WDs. The recent observational study by Hunt et al. (2018a, 2018b, 2019a, 2019b, and 2021) found a westward tilt with height, which implies a northward transport of sensible heat (V'T' > 0) as explained below. They seem to have neglected this important implification.

Assume a perturbation in the stream function Ψ (primes are omitted for simplicity)

$$\phi = A(P,t)\,sinkx + B(P,t)\,coskx$$

$R_\phi(P,t)\,sin(kx+\delta(P))_y$; $\vartheta = \frac{\partial\phi}{\partial x} = Rcos(kx+\delta)$ — (1)

$$\frac{\partial \varnothing}{\partial P} = f\frac{\partial\phi}{\partial P} = f\frac{\partial R}{\partial P}sin(kx+\delta) + fRcos(kx+\delta)\frac{\partial\delta}{\partial P}$$

So, $\vartheta\frac{\partial\varnothing}{\partial P} = R^2 fkcos^2 kx + \delta\frac{\partial\delta}{\partial P} + Rf\frac{\partial R}{\partial P}sin(kx+\delta)cos(kx+\delta)$

Taking zonal average

$\vartheta\frac{\partial\varnothing}{\partial P} = \frac{f}{k}\,\dot{\vartheta}^2\,\frac{\partial\delta}{\partial P}$ since $\vartheta = Rcos(kx+\delta)$

Or $\vartheta\left(\frac{-RT}{P}\right)=\frac{f}{k}\,\vartheta^{2}\,\frac{\partial\delta}{\partial P}$ as$\left\{\frac{\partial\varnothing}{\partial P}=-Z=\frac{-RT}{P}\right\}$

Or $\vartheta T=\frac{-Pf}{R}\,\vartheta^{2}\,\frac{\partial\delta}{\partial P}-(2)$

If the trough or ridge tilt westward with height as observed by the Hunt et al. (2018a) $\frac{\partial\delta}{\partial P}<0$, $\vartheta T>0$ or northward transport of the sensible heat.

Also, for a simple quasi-geostrophic atmosphere, the energy exchanges can be derived (see Holton 2014 for more details) as

$\frac{\partial K}{\partial t}=C\left(P,K\right)-(3)$

$\frac{\partial P}{\partial t}=C\left(P_{z},P\right)-C\left(P,K\right)-(4)$

Where C(P, K) is the rate of conversion between the available potential energy of the eddy and eddy kinetic energy given by

$C\left(P,K\right)=\int\omega T\,dm-(5)$

$C\left(P_{z},P\right)=-\int\frac{R}{P\sigma}\frac{\partial U}{\partial P}\,\vartheta T\,dm-(6)$

From Eq. (6), we note that if there is a northward transport of sensible heat by WD ($\vartheta T>0$) for vertically increasing subtropical westerlies i.e. i.e., $\frac{\partial U}{\partial P}<0$, then $C\left(P_{z},P\right)>0$. This means that mean available potential energy gets converted into perturbation (for WDs) kinetic energy.

Also, for warm air rising and cold air sinking zonally, $C\left(P,K\right)>0$.

That is, the energy cycle of WD would be:

$P_{z}\rightarrow P\rightarrow K$ - (7)

Equation (7) is the typically unstable perturbations energy cycle found for WD by Rao and Rao (1971). In the case of WD, Hunt et al. (2018a) found a westerly tilt with a height that is P_{z}, ÜiPoccurs. But, in their Figures of anomalies Fig. 4, the waves with warm air rising and cold air sinking are not clear. If they had shown actual temperature values instead of anomalies, they might have seen warm air raising in front of the WD and cold air sinking behind the WD trough.

The perturbation quasi-geostrophic omega equation can be derived as

$\frac{\partial^{2}\omega}{\partial x^{2}}+\frac{f_{o}^{2}}{\sigma}\frac{\partial^{2}\omega}{\partial P^{2}}=\frac{f}{\sigma}\left[2\frac{\partial U}{\partial P}\frac{\partial}{\partial x}\left(\frac{\partial^{2}\psi}{\partial x^{2}}\right)+\beta\frac{\partial\vartheta}{\partial P}\right]-(8)$

Where symbols have usual meaning. Then if we make the following simplification

$\frac{\partial^{2}}{\partial x}=\frac{-1}{L^{2}}\,;\frac{\partial^{2}}{\partial x}=\frac{-1}{P^{2}}-(9)$

Also, for a simple quasi-geostrophic atmosphere

$$\omega=\frac{fp^{2}}{\sigma p^{2}+L^{2}p^{2}}\left[2\frac{\partial U}{\partial P}\vartheta-\beta L^{2}\frac{\partial\vartheta}{\partial P}\right]$$

For waves of wavelength for WD (small scale waves), the second term, the *beta* in the bracket, can be neglected because L square is small, Then

$$\omega=\frac{fp^{2}}{\sigma p^{2}+L^{2}p^{2}}\left[2\frac{\partial U}{\partial P}\vartheta\right]$$

Ahead of WD ϑ>0 and $\frac{\partial U}{\partial P}$ is negative for the subtropical jet with strong westerlies and vertical shear i.e.,œâ<0. On the other hand, ahead of the trough, there would be a raising motion, as observed by Hunt et al. (2018a). This shows that WD has all the typical characteristics of baroclinically unstable wave disturbances, as earlier discussed by Rao and Rao (1971).

4. Results And Discussion

The cyclone track density based on the MSLP for all the four seasons: Winter, Spring, Summer, and Autumn of NH is illustrated in Fig. 1. During boreal winter, we note two well-known STs in the Atlantic and Pacific Oceans (Blackmon 1976), with the Atlantic ST being stronger and extending meridionally towards the pole and longitudinally towards the East. In addition, there is an isoline of track density (TD) covering the entire hemisphere, except Alaska at the polar latitudes. During the winter, the centre of TD is observed over eastern Europe. In the spring, the same features are observed, but with less TD of the Atlantic ST and a slight increase in TD over Siberia. The TD of the Atlantic ST over the northern United States of America (USA) and Canada increases in the summer, while the ST over Siberia weakens. ST over Siberia increased in TD in autumn, and it was very similar to that in the spring season.

Figure 2 depicts the TD for cyclonic relative vorticity at 1000 hPa. In winter, TD is very strong in the western Atlantic region and across eastern Europe. The eastward and poleward shift is also seen but somewhat different from that at MSLP (see Fig. 1). During the spring, similar features are noted, with a slight drop in TD in the west Atlantic and East European regions. In summer, the Atlantic ST did not weaken much, but the Pacific ST was weaker. In autumn, the TD of STs has increased again both in the Atlantic and Pacific regions. In autumn and spring, the TD structure of STs and their intensity are similar (see Wallace & Hobbs for a comparison of the transition seasons). Wallace and Hobbs (2006) noted that the STs are stronger during the transition seasons than during the boreal summer.

The TD of cyclonic relative vorticity at 800 hPa in winter (Fig. 2), a careful examination reveals that there are no eastward or westward shifts in the center of Atlantic or Pacific ST, compared to those in MSLP seen earlier, except that they are weaker at 800 hPa level. What is interesting to note at 800 hPa level is a clear TD contours extending over northern India in winter from a maximum center over Middle-East, which shows the WDs moving from the Mediterranean Sea to the Indian region, as observed by Hunt et al. (2018a), and these WD are not seen in MSLP distribution. Interestingly, they seem to be generated further upstream over the Middle East (because higher TD is seen here) and then move downstream along the westerlies. We note that these WDs can be traced only at 800 hPa. In spring also (Fig. 3b), these can be observed, but the TD is lower. In our present study of STs, these WD are noted for the first time. Additionally, the Pacific ST is extended westward with two branches over eastern Russia and China at 800 hPa level up to 90°E, not seen at 1000 hPa level. The northward branch is stronger. It seems that as these synoptic systems move southeastward, they intensify further downstream between 150 ° E and 180°E, at the 800 hPa level. Both in the Atlantic and Pacific ST, the TD values are weaker in spring at the 800 hPa level.

Figure 3c shows the TDs at the 800 hPa level in summer. In this season, STs seem to be weakest in the Atlantic sector, but the Pacific ST in the west is stronger than in spring. But, in the Russian region, the TD of ST is weak. The ST depicting the WD is not seen in the Mediterranean Sea, Caspian Sea and Black Sea. Thus, WDs seem to be restricted to winter and spring seasons only. In autumn, Fig. 3d, both the Atlantic and Pacific STs start intensifying, with the two maxima in the west and east sectors. The western Atlantic ST is strongest in winter.

In the winter season at 500 hPa (Fig. 4a), the ST representing WD is strongest and part of the circumpolar ST. Although there seems to be a center of origin in the Middle East region, the ST is much stronger further east and extended furthermore to the east. A careful examination shows three centers of maximum TD. It is unclear whether the WD generated over the Middle East intensified further downstream. The Pacific and Atlantic STs seem to be more extended.

In spring (Fig. 4b), the ST representing WD seems to be cut off from the one over the Middle East. Both the Pacific and Atlantic STs weakened but continue to be circumpolar. In summer (Fig. 4c), the ST representing WDs is absent. The ST over the Atlantic is more intense than in spring and similar to that in winter in the structure. The Pacific ST is weaker in summer than in winter and spring. In autumn (Fig. 4d), there is a region of ST representing WD but much weaker than in winter and spring. In this season, both Pacific and Atlantic STs start intensifying, the center around 150°W STs is stronger than in the other seasons.

Regarding the ST at 300 hPa in winter (Fig. 5a), the ST representing WD is observed, with a maximum over the Middle East and extending over the India region. We note that the intensity of the TD at 300 hPa over the Indian regions is much weaker than at 500 hPa. The STs over the Pacific and Atlantic are somewhat weaker than at 500 hPa. In spring (Fig. 5b), the ST of WD is still there but weaker than at 500 hPa. In spring (Fig. 5c), the ST over the Atlantic intensified, and the strength was similar to that at 500hPa.The Pacific ST also weakened at 500 hPa in summer. In Autumn (Fig. 5d), the ST representing WD can be seen further north and weaker than in other seasons. Both the Pacific and Atlantic STs are intensified.

Figure 6 depicts STs at 100 hPa level. To our knowledge, STs at this level are not discussed in detail so far. In winter, STs are weakest at this level, but they do exist. STs starting over the east Atlantic and continuing to the east of 90°E can be seen. Whether this ST represents WD or not should be verified with further studies of WD. There is a weak ST over high latitudes to the east of the USA and continuing to the east of the USA at 30 ° N. In spring (Fig. 6b), the ST over the Pacific did not extend to the east of the USA, but the northern Atlantic ST extended from west to the east of the USA, compared to that in winter, the intensity is the same, and the ST is weakest. There is a horse-shoe shape ST over the northwestern USA. Over India and the Middle East, only short regions of STs are seen. In Summer (Fig. 6c), there is a relatively (compared to winter and spring) stronger ST over Russia and extended further east and north up to the west USA. In the autumn (Fig. 6d), the Pacific ST is strongest between 30°N and 60°N.

Now, we make some more theoretical comments regarding the observed features of WD. The origin of WD is in Arabia, North Africa, and the Mediterranean, as shown in Fig. 2 of Hunt et al. (2018a). The wavelength estimated by them is 2000 km (average of type 3a and 3b). From Fig. 4a of Hunt et al. (2018a), the half-wavelength is around 12° longitude and the wavelength around 2400 km. Comparable to the value above, Rao and Rao (1971) were the first to make a theoretical and synoptic study of WD. They found 7000 km for the most unstable disturbance for an adiabatic study. From the synoptic study, they estimate a wavelength of about 6000 km. For a two-layer model, Holton (2004, Chap. 6) found 4000 km for a vertical shear of 8 m sec^{-1} between 750 and 250 hPa levels. However, Staley (1986) strongly criticized the use of a low vertical resolution of two levels only. But, for the Eady (1949) continuous atmosphere, Holton (2014) found the most unstable wavelength as 5500 km. These values are much higher than those found by Hunt et al. (2018a).

After WD, Rao and Rao (1971) made their study for the boreal winter season. To find out the seasonal variation in the occurrence of WD, Hunt et al. (2018a) made their Fig. 3. We find WD occurs mostly from January to April, then decreases in number to a minimum in July and August. Then, they started increasing again in December. To investigate the genesis of WD, we further plotted EGR (Fig. 7) for different seasons, namely DJF (Fig. 7a), MAM ((Fig. 7b), and JJA (Fig. 7c), and SON (Fig. 7d) for the period 1980–2020. In Fig. 7a, we find two regions with the highest EGR, indicating genesis regions over the Arabian Peninsula (AP), Iran, and extending to the western Pacific. In the case of MAM, there are three weak EGR regions: northern Africa, northern AP, and northeastern Iran. Only weak EGR is observed in JJA north of Iran at 40° N and over northeastern China. In SON, EGR spans larger area from the middle of China to the western Pacific. Thus, the eastern ST over eastern China, the western pacific, and the ST representing WD are strongest in the boreal winter months of DJF. Another feature of interest is that in winter over northern Africa, ST continues with reasonably high EGR values increasing downstream over

eastern China and the West Pacific with the highest EGR. These features of seasonal variation in genesis found with EGRtheoretically, agree very well with observational characeristics noted by Hunt et al. (2018a).

4.1. Theoretical relation between storm tracks and western disturbances

In this section, we link the observed storm tracks and western disturbances with the theoretical aspects. From Fig. 2a of Hunt et al. (2018a), one can infer a downstream increase of the number of WD from Arabia to the west of India, suggesting a genesis or the occurrence of instability over this region as inferred above with EGR. Hunt et al. (2018a) found a vertical structure of about 2K warm anomaly centred at 200 hPa, above a 3K cold anomaly around 500 hPa. This structure is different from that of a mature mid-latitude baroclinic cyclone, with warm anomaly through the troposphere, but this structure of WD found by Hunt et al. (2018a) is similar to “Medicanes” (Mediterranean Hurricanes, Emanuel 2005). These Medicanes move further East and become WD (Madhura et al., 2015), interacting with highly baroclinic westerly Jet. Thus, the observed WD have a substantially lower tropospheric wet anomaly co-located with raising motion, as found by Hunt et al. (2018a). Further, the observed WD are associated with rainfall, resulting from the raising of humid parcels. This indicates that one should treat these WD as moist baroclinic disturbances. Their wavelength given by Hunt et al. (2018b), we recall, is around 2000 km, much less than that expected from dry baroclinic instability found by Rao and Rao (1971), around 6000 km. These observed WD can be categorized as intermediate-scale disturbances.

In a theoretical study, Bonatti and Rao (1987) studied the moist baroclinic instability of these intermediate-scale disturbances. Bonatti and Rao (1987) make a systematic study of moist baroclinic instability and found 20 vertical layers are sufficient to reproduce satisfactorily, the analytical mathematical results of Mak (1981). Bonatti and Rao (1987) found the most unstable wavelength compatible with several observations is around 2000 Km. The vertical shear, latitude, and static stability of the radiosonde sounding used by them are very similar to the case of WD. Thus, the intermediate -scale (around 2000 Km) observed by Hunt et al. (2018b) can be explained as those resulting from moist baroclinic instability. Therefore, we can conclude the observed WDs are generated by moist baroclinic instability.

5. Summary And Conclusions

In this section, we shall give a brief summary and conclusions of our study on ST and WD in the northern hemisphere. In our present paper, we extend the previous studies that examined ST at two tropospheric levels only, 250 and 850 hPa (Hoskins and Hodges, 2019). Here we study ST at MSLP, 1000 hPa,800 hPa, 500hPa, 300hPa, and 100 hPa levels in all four seasons, winter, spring, summer, and autumn. Further, we emphasize the characteristics of WD, giving a theoretical explanation of the structure, namely the vertical westward tilt with height indicating northward transport of sensible heat and warm air rising and cold air sinking indicating the typical energy conversions of mean available potential energy to perturbation potential energy and perturbation available potential energy to perturbation kinetic energy. This inferred Lorenz energy cycle is similar to the baroclinically unstable perturbation, agreeing with the first theoretical and synoptic study of Rao and Rao (1971). Further, we noted the observed wavelength of WD by hunt et al. (2018a) is around 2000 km, much less than that obtained for the most unstable *dry* baroclinic waves, by Rao and Rao (1971), also by Holton (2014) for both two-layer models and also even for continuous Eady wave, which is around 6000 km. We could successfully explain this important quantitative difference by accounting for the liberation of latent heat of condensation in moist baroclinic instability, which Bonatti and Rao (1987) carefully studied, whose wind and temperature profiles are very similar to those for the WD. Thus, we can conclude that the observed WD over Indian longitudes were developed by moist baroclinic instability of westerlies in north India with associated rainfall.

Another novelty we tried here is to give all observed characteristics of both ST and WD in a table. Thus, a careful look of our table gives the vertical and seasonal variation. Briefly, WD is not observed in the lower levels of MSLP and 1000 hPa. At 800 hPa, they are found with a strength of 40–50 units over the Mediterranean and moving downstream along the westerlies. At 500 hPa, they become stronger with 60–70 units. At 300 hPa, continuous contours are found from 90 E to 150 E with 50–60 units. At 100 hPa, they become weaker but exist with 10–20 units.

This study mainly focuses on the NH STs during Summer, Winter, Spring, and Autumn, extending from the lower troposphere to the lower stratosphere during the 1979–2014 period. In an earlier paper, Hoskins and Hodges (2019) have shown some of the characteristics of ST during boreal winter. In addition to the tropospheric extent at MSLP, 1000 hPa, 800 hPa, 500 hPa, and 300 hPa, we observed the TD of STs extending into the lower stratospheric region at 100 hPa in all the boreal seasons. At 800 hPa, WD cannot be located in summer and fall. While, at 500 hPa, WD can be identified in autumn over the northwest of India with a maximum of 30–40 units, extending only over a small region. At 300 hPa also, WD can be located in autumn only, over northwest India with again 30–40 units at100 hPa, WD is found.

In the theoretical study by Bonatti and Rao (1987) for the observed wind and temperature profiles (which are similar to the observed ones over northwest India), the maximum growth rate is found for a wave with 2000 km wavelength, which is very similar to that found by Hunt et al. (2018a). Further, they found a westward tilt with height in the stream function, again very similar to that found by Hunt et al. (2018a) for the observed WD. Bonatti and Rao (1987) further found that the phase difference between temperature and vertical velocity is such that warm air is rising and cold air is sinking in the zonal plane, indicating perturbation available potential energy is getting converted into perturbation kinetic energy, very much similar to that we inferred for observed WD. Thus, we conclude that observed WDs are generated by moist baroclinic instability of westerlies over north India because their characteristics agree well with theoretically/ numerically deduced ones.

We observe that the TD intensity of STs is stronger during boreal winter at 800 hPa, 500 hPa, 300 hPa, and 100 hPa. Also, we note that the STs are meridionally extending from the polar region to 30°N. Similarly, we note these features of STs in the spring and fall seasons with a lower TD intensity value. The crucial aspect of STs observed across the Middle East and, India & Northeast neighborhood continental regions at 500 hPa, 300 hPa & 100 hPa during winter is the similar period of WD occurring to cause extreme precipitation. As in the earlier section, we have clearly discussed that baroclinic instability is the

triggering mechanism and a common physical phenomenon of STs and WDs. Here, we suggest that the WD observed during the fall and winter seasons is a component of STs observed. This changes the entire perspective of observation of WD during boreal winter, causing extreme precipitation over the Indian region. To understand the impact of climate drivers on lower stratosphere STs and their implications, apart from the tropospheric observations, there is a need for a detailed analysis for the lower stratospheric STs impacts on tropical and mid-latitude weather.,.

Most of the above-mentioned studies on WD's are mainly pure descriptions of observed characteristics (studies by Hunt and others). These studies are necessary, but they remain incomplete, unless various observed features are connected to a theory that explains these features. We now make in the present investigation such an attempt through the "Baroclinic Instability" theory for a quantitative comparison between observed and theoretical characteristics. To our knowledge, this is the first time that a careful theoretical study of WD has been done such that the theoretical/numerical characteristics of the most unstable wave agree well with observed features of WD. Model studies were used/ made to explain the characteristics of WDs but they didn't discuss the theoretical nature of WDs (Hunt et al., 2019a). Thus, our present study is necessary to fill the gap between observed and theoretical characteristics of WD's.

In our present investigation, we could successfully explain the similarity between the observed and theoretical models. For any attempt to predict the origin and development of WD's and ensuing weather, our investigation is inevitable. Once the quantitative similarity between observed and theoretical features is achieved, then formal attempts can be made for prediction through Numerical Weather Prediction, using these theoretical models. This will be the next stage.

This exactly is the philosophy of K, U and M approach discussed above. Our present investigation is a continuation of the simple theoretical and observational study made by Rao and Rao (1971) more than 50 years ago. Here we could achieve some success in understanding (U) (i.e., understanding the nature of WD theoretically) part of K, U and M approach. We emphasize that this theoretical understanding is crucial to achieve accurate prediction as stressed by Prof. K. Emanuel (2020) and Prof. A.D. Gill (1985).

Declarations

Acknowledgments

We acknowledge the cyclone tracking algorithm from Hodges (199*). Authors gratefully acknowledge ECMWF and NCEP-NCAR reanalysis data base.

Data Availability Statement

All the data used in this study is publicly available and accessible.

Authors' Contributions

VBR conceptualized the idea. VBR and RA wrote the manuscript. HP carried out scientific and statistical analyses. VSLB, SSVS, DG, MAG, KA & KJR shared valuable comments and carefully evaluated the manuscript.

Conflict of Interest

The authors declare that they have no conflict of interest.

Competing Interests

The authors declare no competing interests.

Ethics declarations:

The authors understand their ethical responsibility towards the present submission. There is no violations to the ethics as mentioned by Springer publications.

References

1. Ashok, K., H. Nakamura, and T. Yamagata, 2007: Impacts of ENSO and Indian Ocean Dipole events on the Southern Hemisphere storm-track activity during austral winter, J. Clim., 20, 3147–3163.
2. Ashok, K., C. Tam, W.J. Lee, 2009: ENSO Modoki impact on the Southern Hemisphere storm track activity during extended austral winter. Geophy. Res. lett 36(12). https://doi.org/10.1029/2009GL038847.
3. Attada, R., H.P. Dasari, R.K. Kumar, S. Langodan, N.K. Kumar, O. Knio, and I. Hoteit, 2020: Evaluating cumulus parameterization schemes for the simulation of Arabian Peninsula winter rainfall. J. Hydrometeorol., 21, 5, 1089–1114.
4. Blackmon, M. L., 1976: A climatological spectral study of the 500 mb geopotential height of the Northern Hemisphere. J. Atmos. Sci., 33, 1607–1623.
5. Blackmon, M. L., J. M. Wallace, N.-C. Lau, and S. L. Mullen, 1977: An observational study of the Northern Hemisphere wintertime circulation. J. Atmos. Sci., 34, 1040–1053.
6. Bonatti, J.P., and V.B. Rao, 1987: Moist Baroclinic Instability in the Development of North Pacific and South American Intermediate-Scale Disturbances. J. Atmos. Sci, 44 (18). 2657–2667. doi:10.1175/1520-0469(1987)044<2657:mbiitd>2.0.co;2
7. Brahmananda Rao, V., S. Trivikrama Rao, 1971: A theoretical and synoptic study of western disturbances. *PAGEOPH* 90, 193–208 (1971). https://doi.org/10.1007/BF00875523.

8. Charney, J. G., 1947: The dynamics of long waves in a baroclinic westerly current. J. Meteor., 4, 135–162.
9. Dias da Silva, P.E., K.I. Hodges & M.M. Coutinho, 2021: How well does the HadGEM2-ES coupled model represent the Southern Hemisphere storm tracks? Clim Dyn 56, 1145–1162. https://doi.org/10.1007/s00382-020-05523-9.
10. Dimri, A.P, D. Niyogi., A.P. Barros, J. Ridley, U.C. Mohanty, T. Yasunari, D.R. Sikka. 2015: Western disturbances: A review. Rev. Geophys. 53: 225–246.
11. Eady, E. T., 1949: Long waves and cyclone waves. Tellus, 1, 33–52.
12. Guo, Y., E. K. M. Chang, and S. Leroy, 2009: How strong are the Southern Hemisphere storm tracks? Geophys. Res. Lett., 36, L22806, doi:10.1029/2009GL040733.
13. Hartmann, D. L. 1974. Time Spectral Analysis of Mid-Latitude Disturbances, Mon. Wea. Rev., 102(5), 348–362.
14. Holton 2014: An Introduction to Dynamic Meteorology Fifth edition J R Holtan.
15. Hoskins, B. J., and K. I. Hodges, 2002: New perspectives on the Northern Hemisphere winter storm tracks. J. Atmos. Sci., 59, 1041–1061.
16. Hoskins, B. J., & Hodges, K. I. 2005. A New Perspective on Southern Hemisphere Storm Tracks, J. Clim, 18(20), 4108–4129.
17. Hoskins, B. J., & Hodges, K. I. 2019. The Annual Cycle of Northern Hemisphere Storm Tracks. Part I: Seasons, J. Clim, 32(6), 1743–1760.
18. Hunt, K. M. R., J. Curio, A. G. Turner, and R. Schiemann, 2018a: Subtropical westerly jet influence on occurrence of western disturbances and Tibetan Plateau vortices. Geophys. Res. Lett., 45, 8629–8636,
19. Hunt, K. M. R., A. G. Turner, and L. C. Shaffrey, 2018b: The evolution, seasonality, and impacts of western disturbances. Quart. J. Roy. Meteor. Soc., 144, 278–290, https://doi.org/10.1002/qj.3200.
20. Hunt, K. M. R., Turner, A. G., & L. C. Shaffrey, 2019a: Representation of Western Disturbances in CMIP5 Models, J. Clim, 32(7), 1997–2011.
21. Hunt, K. M. R., Turner, A. G., & L. C. Shaffrey, 2019b: Falling Trend of Western Disturbances in Future Climate Simulations, J. Clim, 32(16), 5037–5051.
22. Hunt, K. M. R., Turner, A. G., and R. K. H. Schiemann, 2021. How Interactions between Tropical Depressions and Western Disturbances Affect Heavy Precipitation in South Asia. *Monthly Weather Review* 149, 6, 1801–1825, available from: < https://doi.org/10.1175/MWR-D-20-0373.1>
23. Kotal, S.D, S.S Roy, S.S. Roy Bhowmik, 2014: Catastrophic heavy rainfall episode over Uttarakhand during 16–18 June 2013 –observational aspects. Curr. Sci. 107: 234–245.
24. Machado, J. P.; Justino, F.; C.D. Souza, 2020: Influence of El Niño-Southern Oscillation on baroclinic instability and storm tracks in the Southern Hemisphere. Int. J Clim, https://doi.org/10.1002/joc.6651.
25. Madhura, R.K., Krishnan, R., Revadekar, J.V. et al 2015: Changes in western disturbances over the Western Himalayas in a warming environment. *Clim Dyn*. 44, 1157–1168 (2015). https://doi.org/10.1007/s00382-014-2166-9.
26. Mak, M., 1981: An inquiry on the nature of CISK. Part I. Tellus, *33*(6), pp.531–537.
27. Nischal S., R, Attada., Hunt, K.M. R. 2022: Evaluating Winter Precipitation over the Western Himalayas in High-Resolution Indian Regional Reanalysis using multi-source climate datasets, Journal of applied meteorology and climatology (under review).
28. Rao, V. B., A. M. C do Carmo, & S. H. Franchito, 2002. Seasonal Variations in the Southern Hemisphere Storm Tracks and Associated Wave Propagation, J. Atmos. Sci, 59(6), 1029–1040.
29. Sawyer, J. S., 1970: Observational characteristics of atmospheric fluctuations with a time scale of a month. Quart. J. Roy. Meteor. Soc., 96, 610–625, https://doi.org/10.1002/qj.49709641005.
30. Wang, J., H. Kim, & E. K. M Chang. 2017: Changes in Northern Hemisphere Winter Storm Tracks under the Background of Arctic Amplification, J Clim, 30(10), 3705–3724.
31. Zhang, L., Gan, B., Wu, L., Cai, W., & Ma, H. 2018: Seasonal Dependence of Coupling between Storm Tracks and Sea Surface Temperature in the Southern Hemisphere Midlatitudes: A Statistical Assessment. J Clim, 31, 4055–4074
32. Zhang B. G, H. Wang, L. Wu, Wenju Cai 2020: Essential Role of the Midlatitude South Atlantic Variability in Altering the Southern Hemisphere Summer Storm Tracks, 47 (17) https://doi.org/10.1029/2020GL087910

Figures

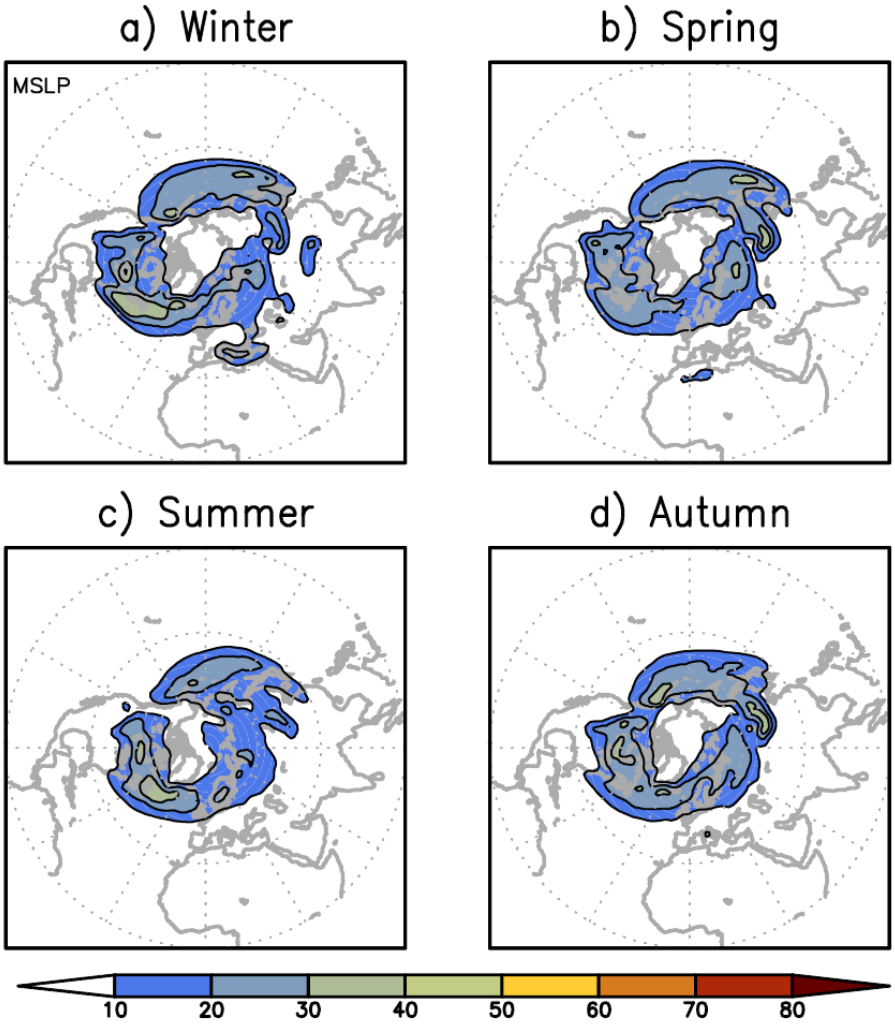

Figure 1

Track density for negative MSLP for boreal seasons for the 1979-2014 period: a) Winter, b) Spring, c) Summer and d) Autumn. Units are number density per season per unit area where unit area is equivalent to 5^{o} radius spherical cap.

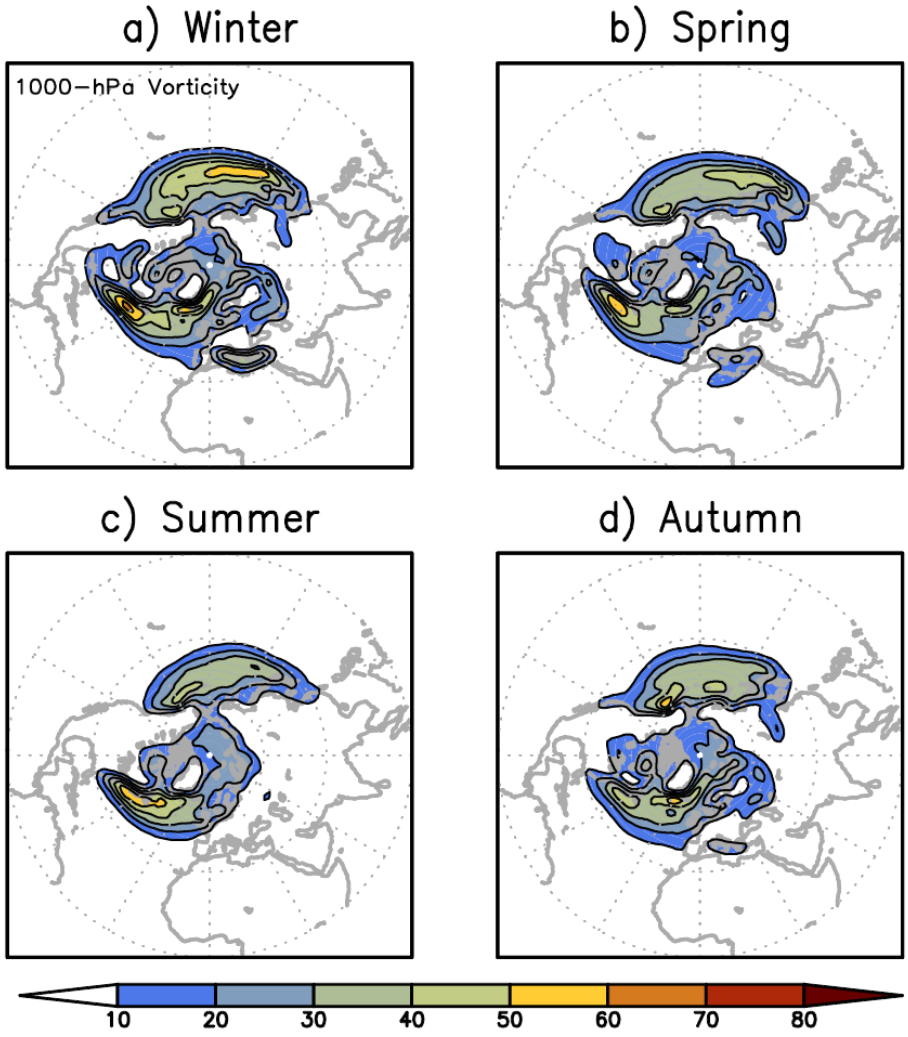

Figure 2

Track density for positive 1000-hPa relative vorticity for boreal seasons for the 1979-2014 period: a) Winter, b) Spring, c) Summer and d) Autumn. Units are number density per season per unit area where unit area is equivalent to 5^{o} radius spherical cap.

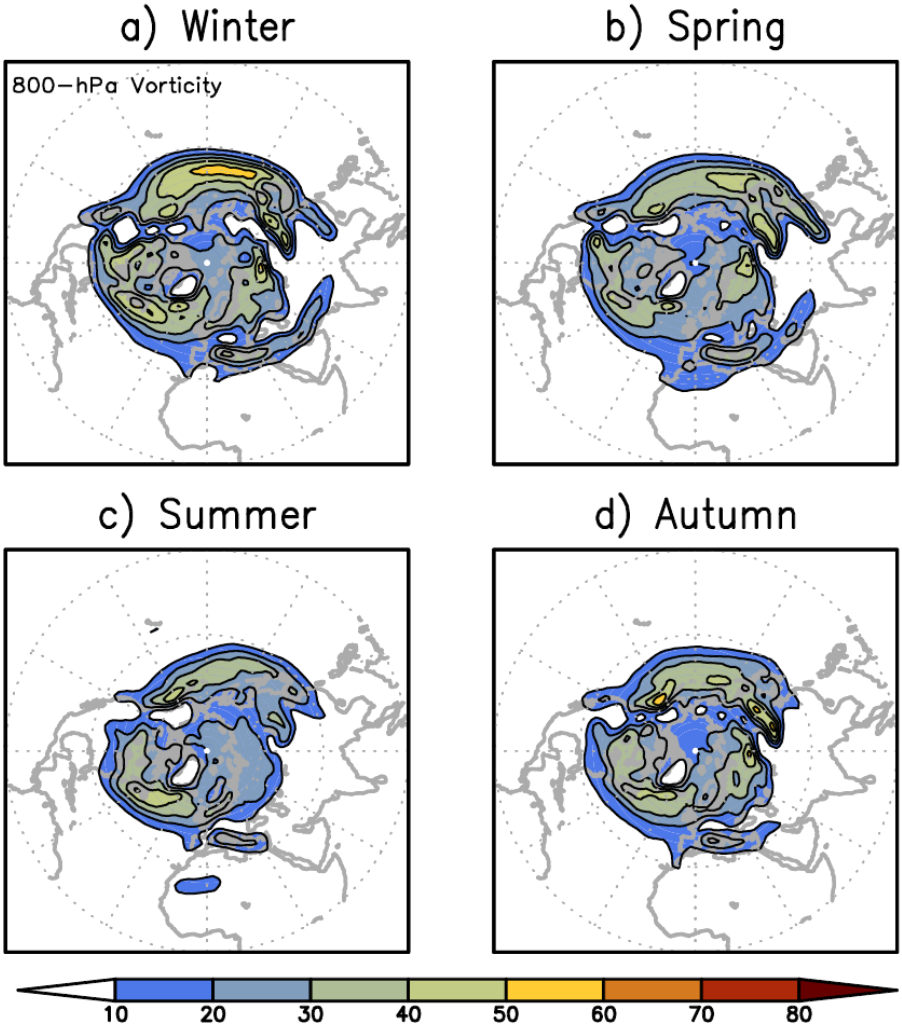

Figure 3

Track density for positive 800-hPa relative vorticity for boreal seasons for the 1979-2014 period: a) Winter, b) Spring, c) Summer and d) Autumn. Units are number density per season per unit area where unit area is equivalent to 5^{o} radius spherical cap.

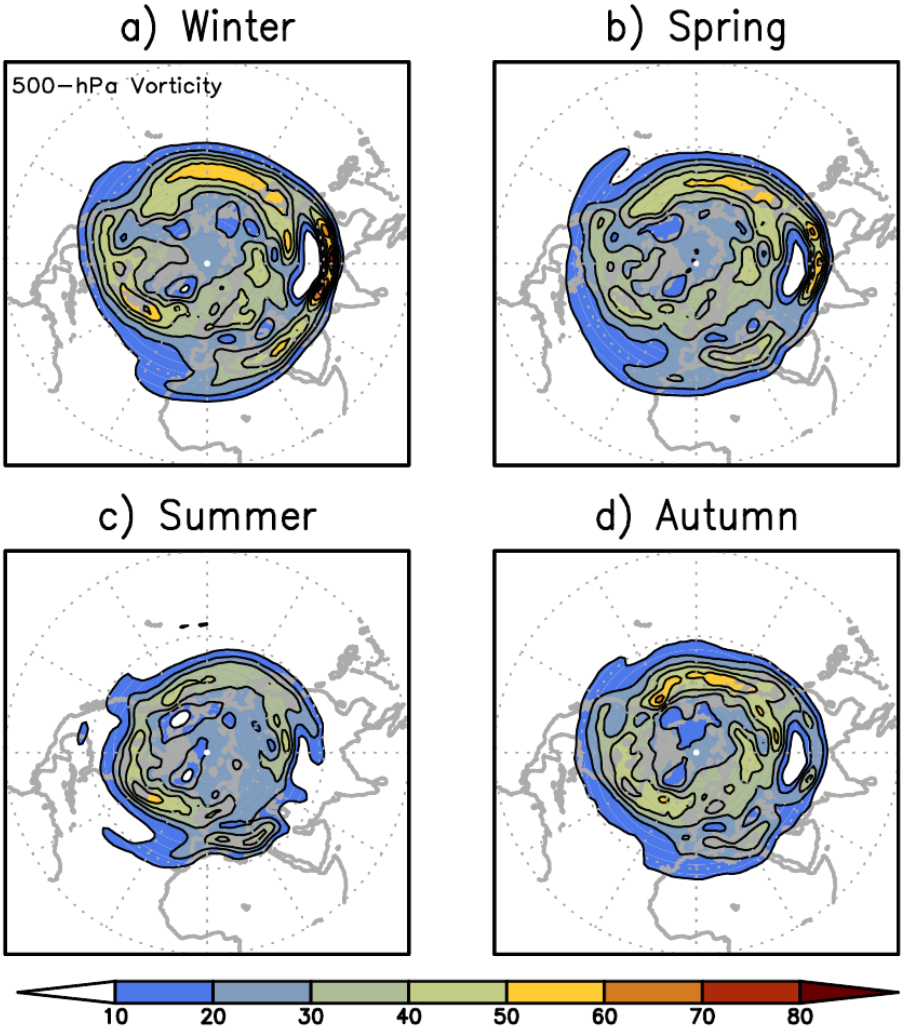

Figure 4

Track density for positive 500-hPa relative vorticity for boreal seasons for the 1979-2014 period: a) Winter, b) Spring, c) Summer and d) Autumn. Units are number density per season per unit area where unit area is equivalent to 5^{o} radius spherical cap.

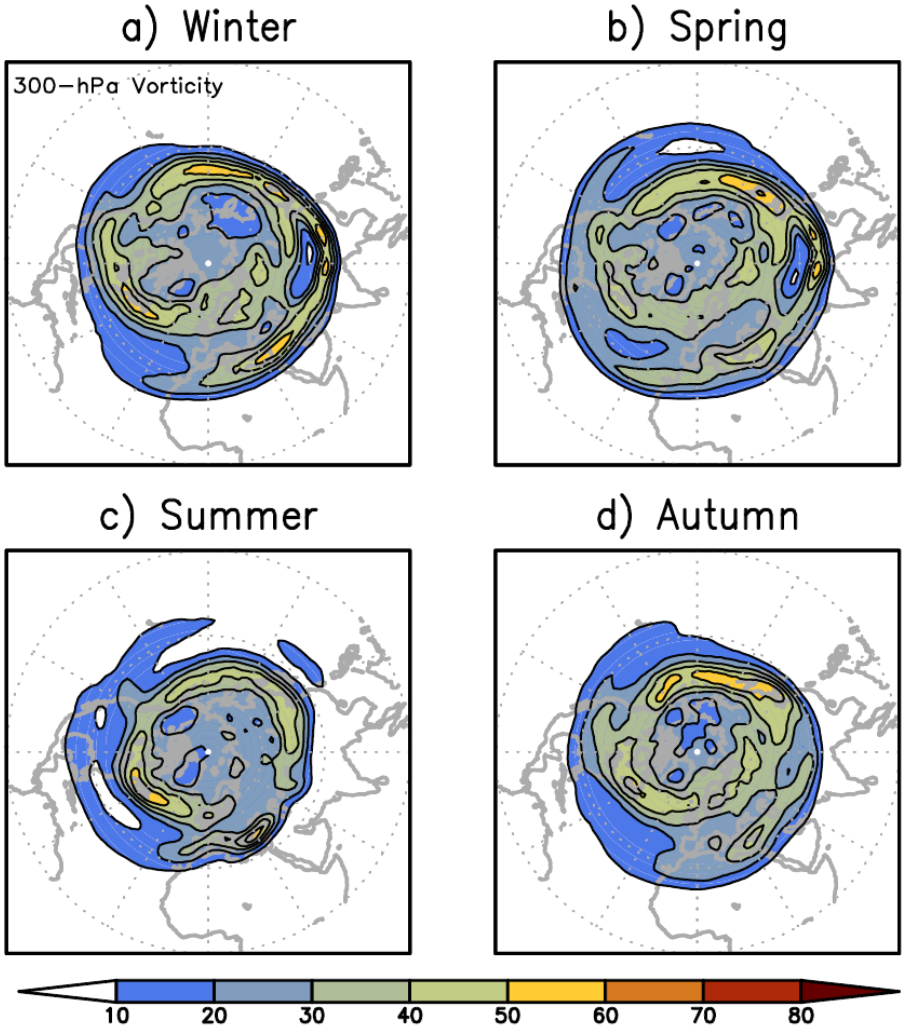

Figure 5

Track density for positive 300-hPa relative vorticity for boreal seasons for the 1979-2014 period: a) Winter, b) Spring, c) Summer and d) Autumn. Units are number density per season per unit area where unit area is equivalent to 5^{o} radius spherical cap.

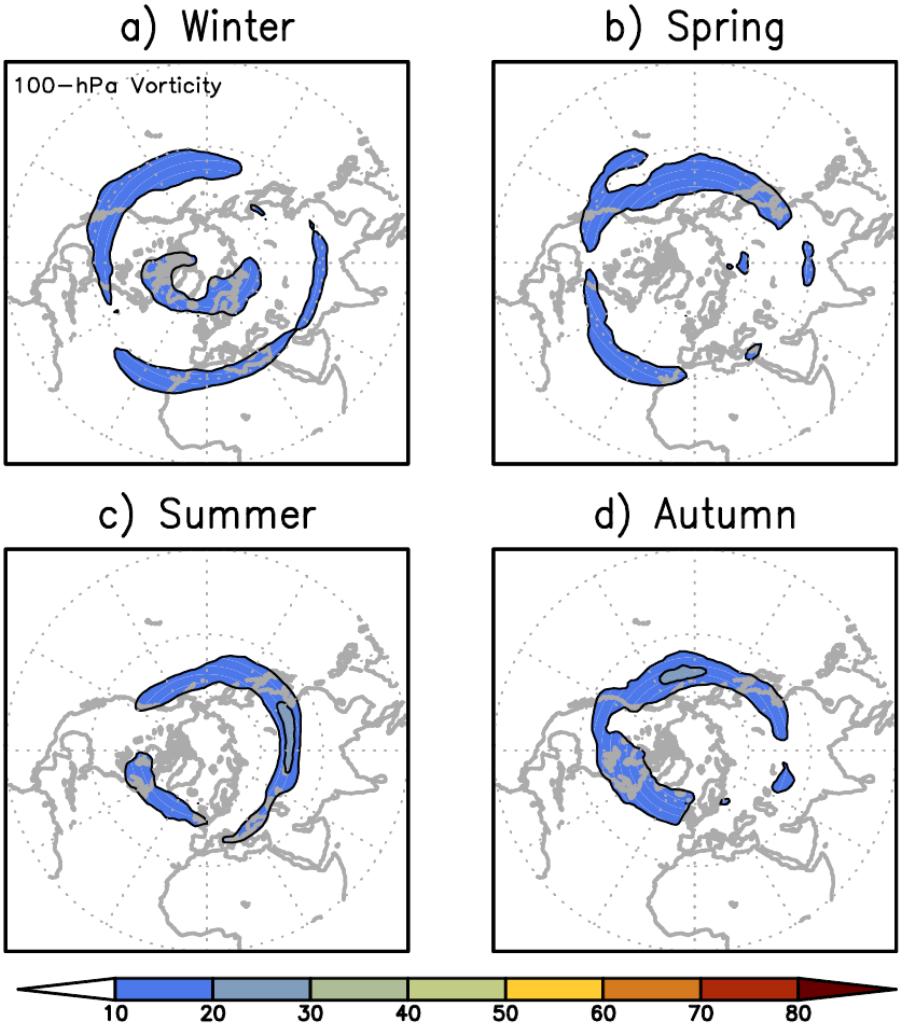

Figure 6

Track density for positive 100-hPa relative vorticity for boreal seasons for the 1979-2014 period: a) Winter, b) Spring, c) Summer and d) Autumn. Units are number density per season per unit area where unit area is equivalent to 5^{o} radius spherical cap.

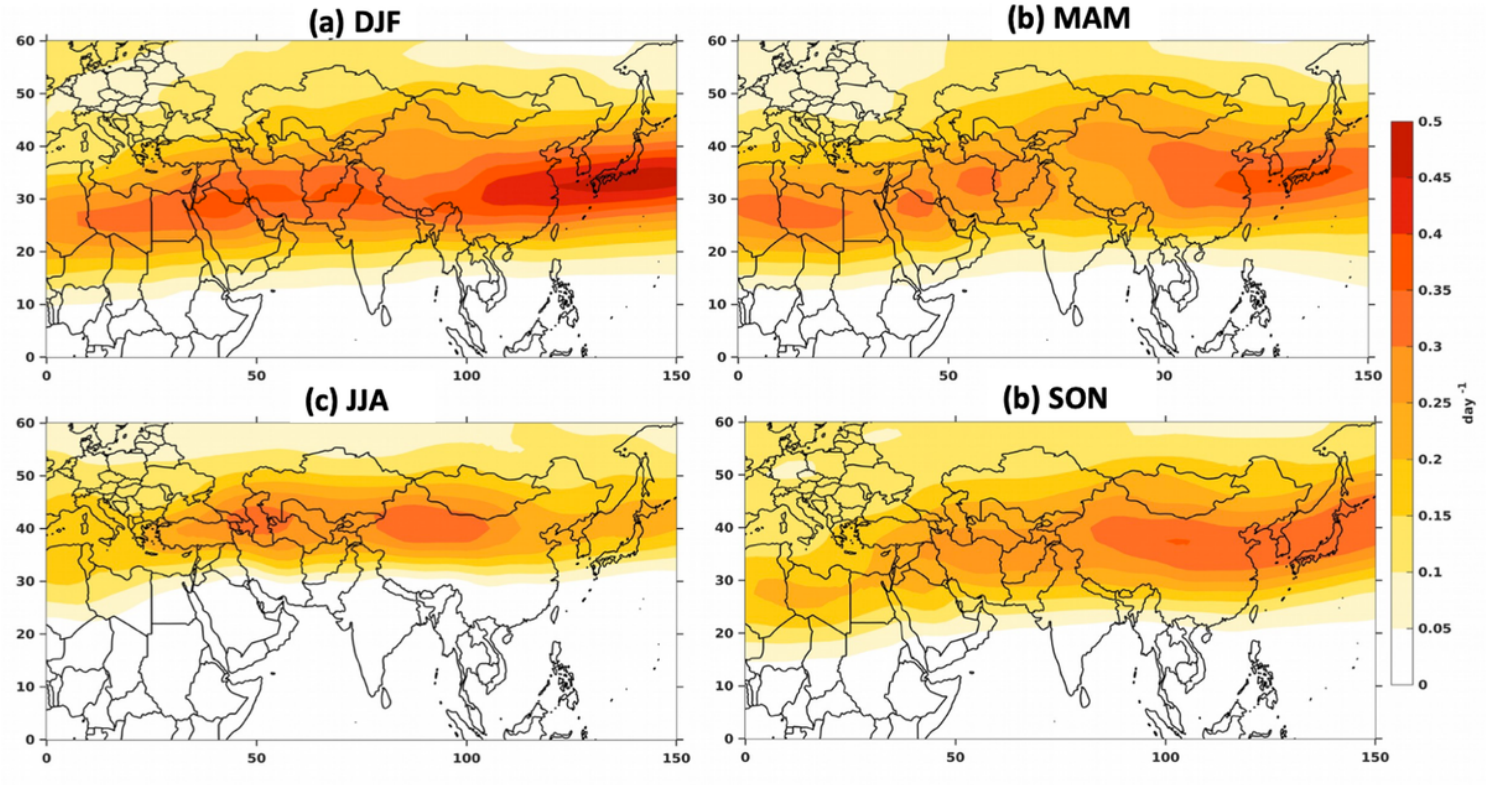

Figure 7

Spatial distribution of seasonal mean Eady growth rate(units in per day) for the period 1980-2020